Batteries & Supercaps

Research Article
doi.org/10.1002/batt.202100339

Chemistry Europe
European Chemical Societies Publishing

www.batteries-supercaps.org

Spinel Type Mn–Co Oxide Coated Carbon Fibers as Efficient Bifunctional Electrocatalysts for Zinc-Air Batteries

Zahra Abedi,[a] Desirée Leistenschneider,[a] Weixing Chen,[a] and Douglas G. Ivey*[a]

Mn–Co mixed oxide nanoparticles were coated onto carbon fibers (CFs) derived from asphaltene through a facile coating process. Homemade gas diffusion layers (GDLs) were prepared with the coated CFs to be employed as air electrodes and bifunctional oxygen reduction reaction (ORR) and oxygen evolution reaction (OER) electrocatalysts for Zn-air batteries (ZAB). The Mn–Co oxide was identified as a cubic spinel phase ($MnCo_2O_4$) by transmission electron microscopy (TEM) and X-ray photoelectron spectroscopy (XPS). The composite air electrode showed excellent catalytic activity towards ORR/OER, outperforming the benchmark Pt-RuO_2 catalyst in both half-cell and full-cell configurations with discharge/charge efficiencies of 63.7% and 60.0% at 10 and 20 mA cm^{-2}, respectively. After 200 cycles (100 h) at 10 mA cm^{-2} the final efficiency of the composite electrode (58.9%) was still superior to that of Pt–Ru (43.2%).

1. Introduction

Zinc-air batteries (ZABs) are considered as a safe and inexpensive energy storage solution as the world becomes less dependent on fossil fuels and moves toward renewable energy technologies. Compared with other commonly used batteries like Pb-acid batteries and Li-ion batteries, ZABs are low cost, non-polluting and safe. They can provide energy densities as high as 1048 Wh kg^{-1}. ZABs are currently used in hearing aids, navigation lights and railway signals. Their limited use is mainly because of their poor cycling behavior and low discharge/charge efficiencies.[1–3]

A metallic zinc electrode, an air electrode and a typical electrolyte, consisting of 6 M KOH and ~0.25 M Zn^{2+}, are the main components of a ZAB. The air electrode is usually carbon based; this electrode is often referred to as the gas diffusion layer (GDL). The oxygen reduction reaction (ORR) and oxygen evolution reaction (OER) take place at the surface of the air electrode during discharge and charge, respectively. Equation 1 shows the ORR; Equation (1) in reverse is the charge reaction (OER).[2,4–7]

$$O_2 + 2H_2O + 4e^- \xrightarrow{\text{discharge}} 4OH^- \quad (1)$$

Nanoscale carbonaceous materials such as graphene nanosheets or powder, carbon nanotubes (CNTs) and nanoscale carbon fibers are usually used to prepare air electrodes. Electrocatalysts are coupled with the air electrode via different methods like electrodeposition or atomic layer deposition (ALD). Preparation steps for these nano-scale carbon-based materials are often costly and time consuming. A cost-effective carbonaceous precursor with a facile preparation method is desirable for preparing air electrodes. Asphaltene is a carbon rich and inexpensive (more supply than demand) by-product of partial upgrading of bitumen extracted from the oil sands. Asphaltene currently has no further value other than low quality fuel or landfill; however, it can be utilized to prepare micron-scale carbon fibers (CFs).[8–18]

Electrocatalysts in the air electrode play a vital role in improving the efficiency and cycling behavior of a ZAB, which tend to be limited by the inherent poor kinetics of the ORR and OER reactions that take place at the air electrode. Transition metal oxides have been employed as ORR/OER electrocatalysts in ZABs as alternatives to precious metals like Pt or Ru. Transition metal oxides, such as Mn, Co, Ni and Fe oxides demonstrate promising bifunctional catalytic activity towards ORR and OER. Their low cost, safety, abundance and ease of handling make them desirable for use as electrocatalysts in ZABs. Co-based transition metal oxides have been shown to demonstrate strong OER catalytic activity, while Mn-based transition metal oxides have good ORR catalytic activity. As such, combining the two oxides into Mn–Co mixed oxides has generated significant interest as bifunctional catalysts for metal-air batteries.[2,14,19–22]

In this work, carbon fibers (8–12 μm in diameter) are prepared through melt-spinning from asphaltene. These fibers are then coated with Mn–Co mixed oxides as bifunctional electrocatalysts for ZABs. Homemade GDLs are prepared, using the coated CFs. This work shows that: 1) costly nano-scale carbonaceous materials are not needed to prepare air electrodes or electrocatalysts, 2) ORR catalytic activity of homemade air electrodes, prepared with asphaltene based CFs (not coated with Mn–Co electrocatalyst), is similar to that of commercially available GDLs while presenting superior OER activity, and 3) Mn–Co mixed oxide coated CFs display comparable or better cycling behavior and efficiency relative to similar metal oxide/carbon based electrodes in the recent literature. These electrodes are fabricated using a cost-effective procedure.

[a] Z. Abedi, D. Leistenschneider, W. Chen, Dr. D. G. Ivey
Department of Chemical and Materials Engineering
University of Alberta
Edmonton, Alberta, T6G 2V4, Canada
E-mail: divey@ualberta.ca

Supporting information for this article is available on the WWW under https://doi.org/10.1002/batt.202100339

Research Article
doi.org/10.1002/batt.202100339
Chemistry Europe
European Chemical Societies Publishing

Experimental

Carbon fiber synthesis

Carbon fiber synthesis was done based on process developed by Zuo et al.[23] and Leistenschneider et al.[24] In a typical procedure, as-received asphaltene powder was processed into asphaltene fibers by a melt-spinning process. Melt spinning was done using an AT255 system from Anytester. Asphaltene powder was melted at 197 °C in a N_2 atmosphere. The soft asphaltene powder was then pressed through a spinneret hole with a diameter of 15 μm and a N_2 gas pressure of 400 kPa and collected on a rotating drum with a speed of 200 rpm. Afterwards, asphaltene fibers were cooled under ambient conditions. A one-step oxidation process was performed on the fibers followed by soaking in 3.2 M HNO_3 for 10 min to prevent melting at elevated temperature. The fibrous material was heated to 300 °C at a heating rate of 1.5 °C min^{-1} and kept at this temperature for 120 min. Oxidized fibers were then divided into three batches; each batch was carbonized at 500 °C (CF-500), 800 °C (CF-800) or 1500 °C (CF-1500) for 2 h in N_2. 1500 °C is the maximum temperature attainable by the furnace.

Electrocatalyst coating synthesis

CF-1500 was chosen as the substrate for Mn–Co mixed oxide coatings due to its superior ORR/OER catalytic activity compared with fibers carbonized at the other temperatures (see discussion in Section 2.1). 80 mg of carbonized fibers (CF-1500) were soaked in 20 mL of 28 wt% NH_4OH for 10 min to introduce N containing groups onto the surface of the carbonized fibers; the aim was to provide nucleation sites for the electrocatalyst coating. The fibers were then sonicated in a mixture of 30 mL of reagent alcohol, 100 mg of NaOH and a 500 mg mixture of Mn(II) acetate ($Mn(Ac)_2$ or $C_4H_6MnO_4$) and Co(II) acetate ($Co(Ac)_2$ or $C_4H_6CoO_4$) salts. The sonication time was varied from 0 h (MnCo-no sonication) to 6 h (MnCo-6 h). The mass ratio of acetate salts, i.e., $Mn(Ac)_2/Co(Ac)_2$, in the sonication solution was 1:1 (250 mg of each salt). The sonication method in this work is similar to the one reported by Li et al.[25] for N-doped carbon nanotubes (N-CNT).

The sonication time that led to the best ORR/OER catalytic activity and full-cell ZAB performance (5 h, discussed in Section 2.2) was chosen to prepare Mn–Co mixed oxide decorated CF-1500. Three mass ratios of acetate salts ($Mn(Ac)_2/Co(Ac)_2$) in the sonication solution were tested, i.e., 2:1 (333.33 mg of Mn salt and 166.67 mg of Co salt), 1:2 (166.67 mg of Mn salt and 333.33 mg of Co salt) and 1:1 (250 mg of Mn salt and 250 mg of Co salt), to investigate the effect of salts ratio. These samples are denoted as MnCo-5h-2:1, MnCo-5h-1:2 and MnCo-5h-1:1, respectively.

Electrode preparation

Carbon fiber electrodes that were carbonized at different temperatures (without Mn–Co mixed oxide) were prepared by pasting a mixture of 90 wt% CF, 5 wt% polytetrafluoroethylene (PTFE) and 5 wt% carbon black onto carbon paper (Fuel Cell Store: Toray Paper 030-TGP-H-030).

Electrodes consisting of Mn–Co mixed oxide decorated CF-1500 fibers were prepared by pasting a mixture containing 90 wt% Mn–Co mixed oxide decorated CF-1500, 5 wt% PTFE and 5 wt% carbon black onto a hydrophobic carbon paper (Fuel Cell Store: Toray Paper 060-TGP-H-060). The carbon paper provided structural support and helped prevent electrolyte leakage during operation. Mass loading for each electrode was ~10 mg cm^{-2} of CF or Mn–Co mixed oxide coated CF-1500.

The electrochemical performance of the prepared electrodes, in both half-cell and full-cell configurations, was compared with electrodes fabricated with Pt-RuO_2 benchmark catalysts (referred to as Pt–Ru in this work).[26] The latter electrodes were spray coated on commercial GDL (Fuel Cell Store: Toray Paper 060-TGP-H-060) with a mass loading of ~0.5 mg cm^{-2}. The spray coating suspension was prepared by mixing 50 mg of Pt-RuO_2 powder (nominally 30 wt% Pt and 15 wt% RuO_2 combined with carbon black, purchased from Alfa Aesar), 1 mL of ethanol, 0.1 mL Nafion 5% and 2 mL of deionized water (DIW).

Materials characterization

The crystal structure of CF was determined by X-ray diffraction (XRD), using a Rigaku Ultima IV system with Cu K_α radiation, a scanning speed of 3° min^{-1} and a step size of 0.05°. Zero background sample holders were utilized. The microstructure and composition of the samples were determined through field emission scanning electron microscopy (ZEISS Sigma 300 VP-FESEM), using both secondary electron (SE) images and energy dispersive X-ray (EDX) analysis. X-ray photoelectron spectroscopy (XPS) (PHI VersaProbe III scanning XPS Microprobe), with a monochromatic Al X-ray source operated at 210 W and a pass energy of 20 eV, was employed to determine the oxidation state of Mn and Co in the Mn–Co mixed oxide coatings. All XPS spectra were calibrated using the C 1s peak at a binding energy of 285.0 eV and the background was fitted using a Shirley approach. Transmission electron microscopy (TEM) and selected area electron diffraction (SAED), using a JEOL JEM-ARM200F microscope operating at an accelerating voltage of 200 kV, was utilized for further microstructural and crystal structure analysis at a finer scale. CHNS elemental analysis, with a Flash 2000 Organic Analyzer, was employed to evaluate the light element composition of the carbon fibers.

Electrochemical measurements

A Biologic VSP potentiostat was used to investigate the ORR and OER catalytic activity of the CFs and Mn–Co mixed oxide coated CFs as well as full-cell ZAB performance. Linear sweep voltammetry (LSV at 5 mV s^{-1}) in a half-cell configuration with a Pt wire counter electrode and Hg/HgO reference electrode (+0.098 V vs. SHE) was utilized to determine the ORR and OER catalytic activity. Galvanostatic cycling with potential limitation (GCPL) at current densities (j) of ±2, ±5, ±10 and ±20 mA cm^{-2} in a full-cell configuration with a 2×6 cm zinc sheet counter electrode was employed to determine the full-cell charge and discharge potentials, potential gaps and efficiencies at each current density and the cycling behavior of the battery. 1 M KOH and 6 M KOH + 0.25 M ZnO were used as the electrolytes for half-cell and full-cell tests, respectively.

Onset potentials for ORR and OER are defined as the potentials at which current densities of −10 and +10 mA cm^{-2} are achieved, respectively. The efficiency of each ZAB cell is defined as the discharge potential divided by the charge potential, i.e., V_{ORR}/V_{OER}, at the same discharge/charge current density. The potential gap is defined as $\Delta V = V_{OER} - V_{ORR}$ and the maximum current density achieved is defined as the current density at −0.5 V vs. Hg/HgO for ORR and at 0.9 V vs. Hg/HgO for OER.

Research Article
doi.org/10.1002/batt.202100339
Chemistry Europe
European Chemical Societies Publishing

2. Results and Discussion

2.1. Carbon Fiber Characterization and Catalytic Activity

XRD patterns for all three CFs correspond to the patterns for natural graphite (Figure 1).[27] The two main peaks at 26.5° and 44.4° can be indexed to the (002) and (101) planes, respectively (PDF#13-0148; hexagonal with $a = 2.462$ Å and $c = 6.701$ Å).[28] These two peaks are the sharpest and the strongest for CF-1500, which means that carbonization at 1500 °C leads to the most graphitized structure with the highest carbon content CFs. It has been shown previously that higher carbonization temperatures for C-based materials lead to increased graphitization.[29] Also, amongst all C-based materials, graphite-based ones (such as carbon nanotubes, sheets and powder) tend to show the best ORR/OER catalytic activity with long term operation stability.[30] In addition, a study by Ross et al. demonstrated that graphitized carbon has a reduced corrosion rate in harsh alkaline electrolytes, which could improve the cycling behavior of a ZAB in alkaline electrolytes.[31] For these reasons, 1500 °C was chosen as the carbonization temperature for the fibers.

Half-cell LSV curves in O_2 saturated 1 M KOH are shown in Figure 2. The ORR and OER activity increase as the carbonization temperature increases, which is related to an increase in graphitization degree. Graphite has been shown previously to provide active sites for ORR/OER.[26] The CF-1500 sample has the highest activity towards both ORR and OER with ORR and OER onset potentials of −0.23 V vs. Hg/HgO and 0.68 V vs. Hg/HgO, respectively. Also, the ORR activity of CF-1500 is comparable to that of commercial GDL. CF-1500 has a lower absolute onset potential than commercial GDL, while commercial GDL has a slightly higher maximum current density than CF-1500 (Figure 2a). The OER activity of CF-1500 is significantly better than that for commercial GDL; CF-1500 has a lower onset potential and a significantly higher maximum current density. The superior OER catalytic activity for electrodes made with CFs compared with commercial GDL is likely due to the presence of S and N containing groups in the CFs which can enhance OER catalytic activity.[32] Both S and N are present in the CF precursor, as reported previously, and the amounts were measured via CHNS analysis (Table SI1).[16,24]

CF-1500 was chosen as the substrate for Mn–Co mixed oxide ORR/OER bifunctional catalysts due to its promising catalytic activity and high graphitization degree (Figure 1).

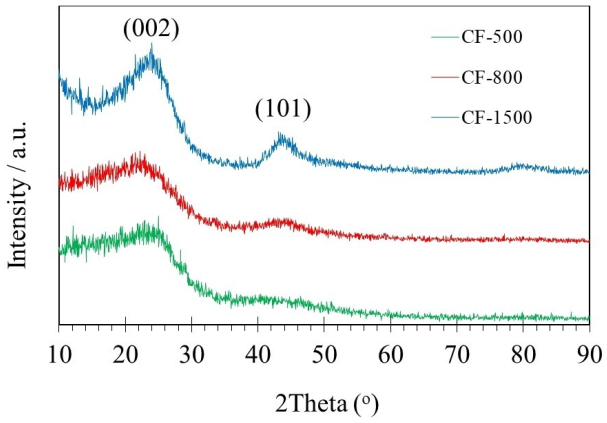

Figure 1. XRD patterns for CFs carbonized at 500 °C, 800 °C and 1500 °C.

2.2. Mn–Co Mixed Oxide Coated Carbon Fiber Characterization and Catalytic Activity

SEM SE images and EDX maps of Mn–Co mixed oxide coated CFs, prepared with no sonication, are shown in Figure 3(a–d) and exhibit a discontinuous coating on the fibers with a particle size in the 1 to 15 μm range. Mn, Co and O signals overlap, which indicates that a Mn–Co mixed oxide was produced. Sonication of the CF-1500 in the salt solution was done in an attempt to improve the quality of the mixed oxide coating on the fibers. The sonication time was varied from 1 to 6 h and the corresponding SEM images and EDX maps are shown in Figure 3. Coating uniformity increased with increasing sonication time; for times 3 h or longer the entire fiber surface is covered with the mixed metal oxide. The oxide coating thickness increases with increasing sonication time, which can cause conductivity and charge transfer issues due to the insulating nature of the oxide.[33] Increasing the sonication time

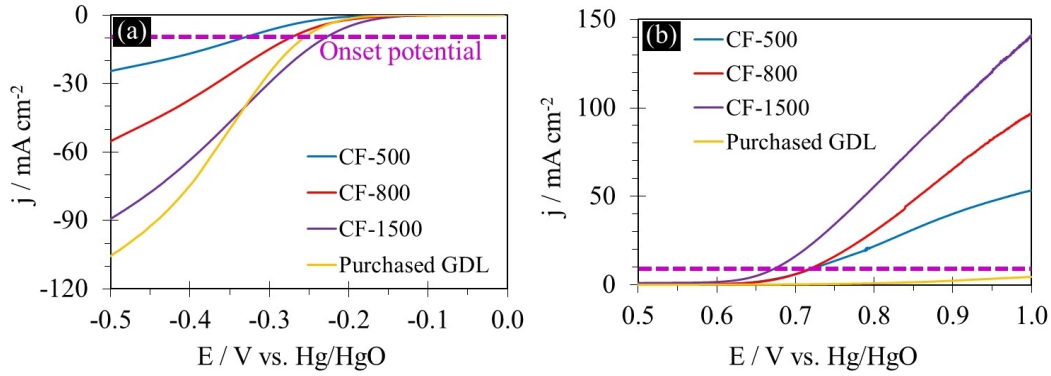

Figure 2. LSV tests at 5 mV s^{-1} showing a) ORR and b) OER catalytic activity of commercial GDL and homemade air electrodes prepared with CF-500, CF-800 and CF-1500.

Research Article
doi.org/10.1002/batt.202100339
Chemistry Europe
European Chemical Societies Publishing

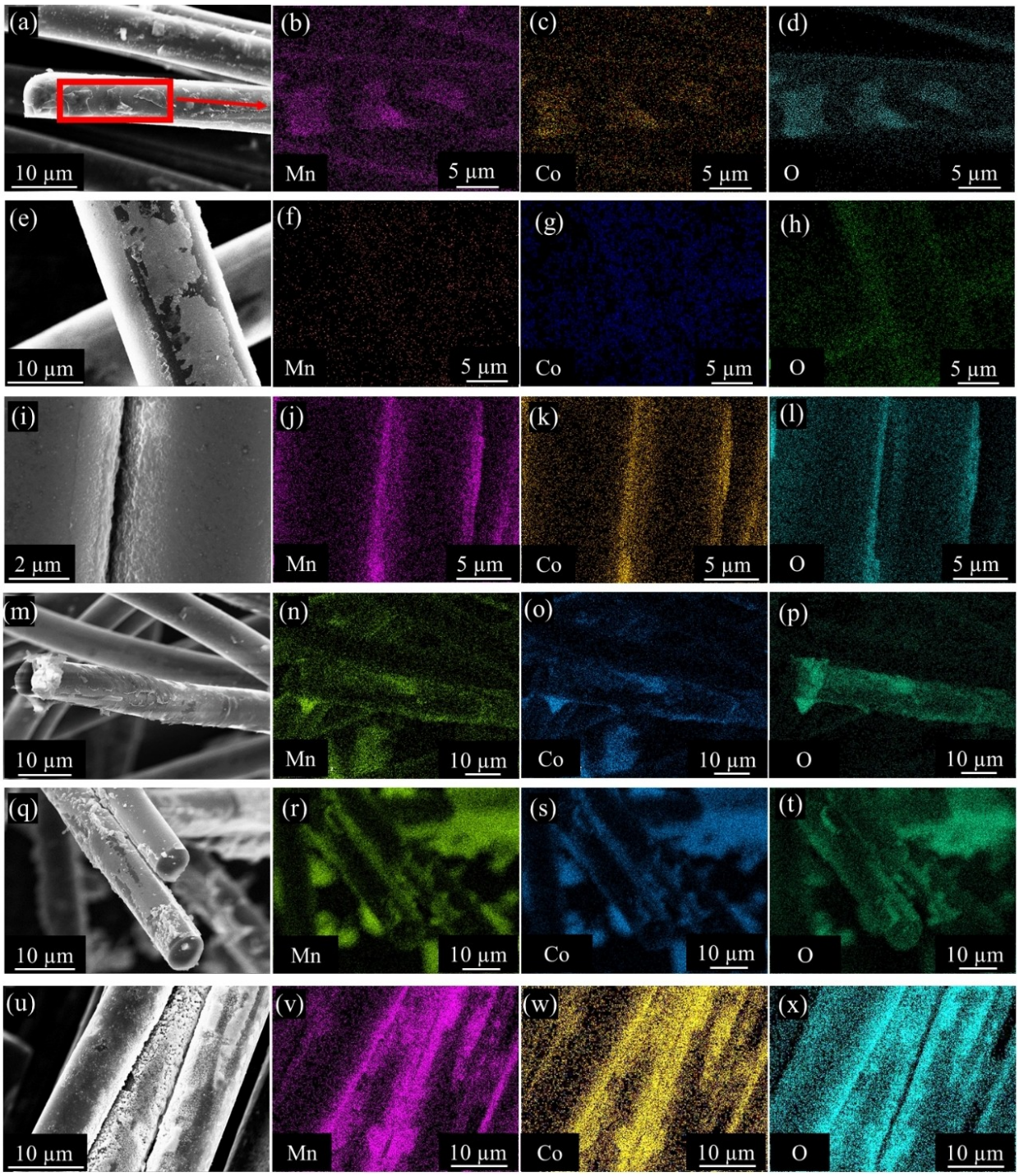

Figure 3. SEM SE images and EDX maps of Mn–Co mixed oxide coated carbon fibers with (a–d) no sonication, (e–h) 1 h, (i–l) 3 h, (m–p) 4 h, (q–t) 5 h and (u–x) 6 h of sonication.

also creates patches of thicker oxide on the surface of the fibers (Figure 3a, e, i, m, q and u). This may not be a major issue in terms of conductivity and electron/species transfer due to the small amount of Mn–Co oxide catalyst relative to the carbon fibers. EDX quantitative analysis (Table 1) was done for each of the areas shown in the SEM images in Figure 3; the sample subjected to 5 h of sonication had the highest amounts of Mn and Co. The amount of Mn-Co oxide coating increases with increasing sonication time up to 5 h and then levels off for longer times (6 h). Longer sonication times may result in some delamination of the oxide coating from the fibers leading to a decrease in the amount of oxide coating. The data in Table 1 indicates that the Mn:Co ratio is close to 1:1 for all samples, with the possible exception of the 4 h sample. The 1:1 ratio corresponds with the Mn:Co ratio of the salts used in the sonication solution.

Research Article
doi.org/10.1002/batt.202100339
Chemistry Europe
European Chemical Societies Publishing

Table 1. EDX quantitative analysis of Mn–Co mixed oxide coated CF-1500.*

Sample	Atomic %			Mass %		
	Mn	Co	O	Mn	Co	O
1 h	0.25	0.25	6.3	1.1	1.2	5
3 h	0.39	0.35	13.2	1.6	1.6	16
4 h	0.51	0.72	10.1	2.1	3.2	12.3
5 h	1.63	1.85	17.6	6.2	7.6	19.5
6 h	1.0	1.0	16.6	4.2	4.2	19.3

*The amount of C, or other residual elements (e.g., S and N), is not included, so the amounts do not add to 100%.

LSV half-cell tests were carried out for the coated fiber electrodes and the Pt–Ru spray coated electrode (Figure 4). Among the sonicated samples, MnCo-5 h has the lowest absolute ORR onset potential of −0.08 V vs. Hg/HgO and the lowest OER onset potential of 0.32 V vs. Hg/HgO (Table 2). These values compare favorably with Pt–Ru, with an ORR onset potential of −0.06 V vs. Hg/HgO and an OER onset potential of 0.63 V vs. Hg/HgO. In fact, the OER onset potential for MnCo-5 h is significantly better than the value for Pt–Ru. MnCo-5 h also has the highest ORR current density of −571 mA cm^{-2} at −0.5 V vs. Hg/HgO. Its maximum OER current density is the lowest (139 mA cm^{-2}) among all sonicated samples, but still exceeds the value for Pt–Ru. The half-cell test results indicate that a sonication time of 5 h is optimal for yielding the most efficient bifunctional electrocatalyst. The MnCo-5 h sample also has the largest amount of Mn–Co oxide coating on the CFs (Table 1).

ZAB full-cell tests were done for the same samples as the half-cell tests (Figure 5) and the behavior is similar to the LSV tests. MnCo-5 h has the best bifunctional catalytic performance among all samples tested including Pt–Ru. MnCo-5 h has a potential gap of 0.74 V and an efficiency of 62.6% at 10 mA cm^{-2}, while Pt–Ru has a potential gap of 0.77 V and an efficiency of 61.9% at the same current density. The potential gap increases to 0.83 V and the efficiency decreases to 58.9% when the current density is increased to 20 mA cm^{-2}. This performance is still better than that for Pt–Ru at 20 mA cm^{-2} (Table 3).

Because of the promising catalytic performance of MnCo-5 h, other electrodes were fabricated by varying the Mn and Co salt composition while maintaining the sonication time at 5 h. The Mn:Co salt mass ratio was changed to 1:2 and 2:1.

LSV half-cell tests were done and the results, including those from the Pt–Ru electrode, are shown in Figure 6. Of the 3 ratios of Mn:Co tested, the sample with a Mn:Co salt ratio of 1:2 has the best ORR (Figure 6a) and OER (Figure 6b) catalytic activity. MnCo-5h-1:2 has a lower absolute ORR onset potential than either MnCo-5h-1:1 or MnCo-5h-2:1 and a maximum

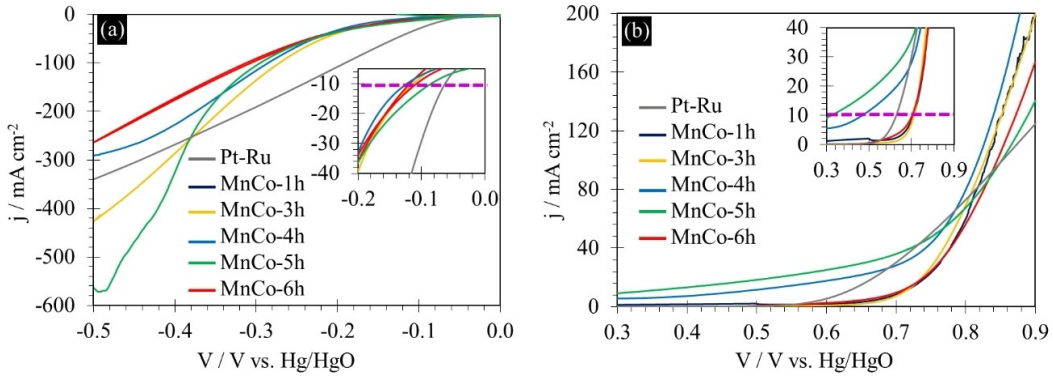

Figure 4. LSV half-cell test results at 5 mV cm^{-2}. a) ORR and b) OER catalytic activities for Mn–Co mixed oxide coated CF-1500 with different sonication times and the Pt–Ru electrode.

Table 2. ORR/OER onset potentials and maximum current densities for Mn–Co mixed oxide coated CF-1500 with different sonication times and Pt–Ru.

Sample	ORR onset potential [V vs. Hg/HgO]	OER onset potential [V vs. Hg/HgO]	Maximum ORR current density [mA cm^{-2}]	Maximum OER current density [mA cm^{-2}]
1 h	−0.14	0.7	−334	200
3 h	−0.11	0.7	−422	200
4 h	−0.12	0.47	−291	199
5 h	−0.08	0.32	−571	139
6 h	−0.11	0.7	−263	167
Pt-Ru	−0.06	0.63	−334	126

Research Article
doi.org/10.1002/batt.202100339
Chemistry Europe
European Chemical Societies Publishing

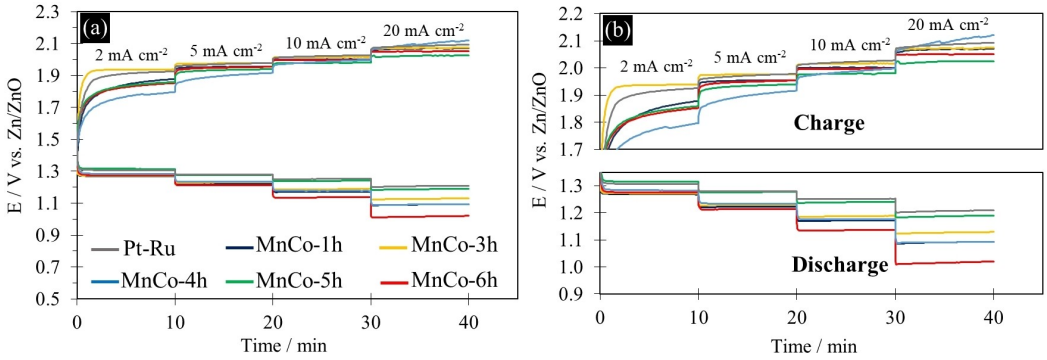

Figure 5. a) ZAB full-cell test results and b) enlarged view of full-cell test results for Mn–Co mixed oxide coated CF-1500 with different sonication times and Pt–Ru.

Table 3. Voltage gaps and efficiencies measured from the full-cell tests for Mn–Co mixed oxide coated CF-1500 with different sonication times and Pt–Ru.

Sample	10 mA cm^{-2}		20 mA cm^{-2}	
	Voltage gap [V]	Efficiency [%]	Voltage gap [V]	Efficiency [%]
1 h	0.83	58.5	0.98	52.7
3 h	0.83	58.9	0.94	54.6
4 h	0.80	59.6	1.01	51.9
5 h	0.74	62.6	0.83	58.9
6 h	0.87	56.5	1.03	49.8
Pt-Ru	0.77	61.9	0.88	57.9

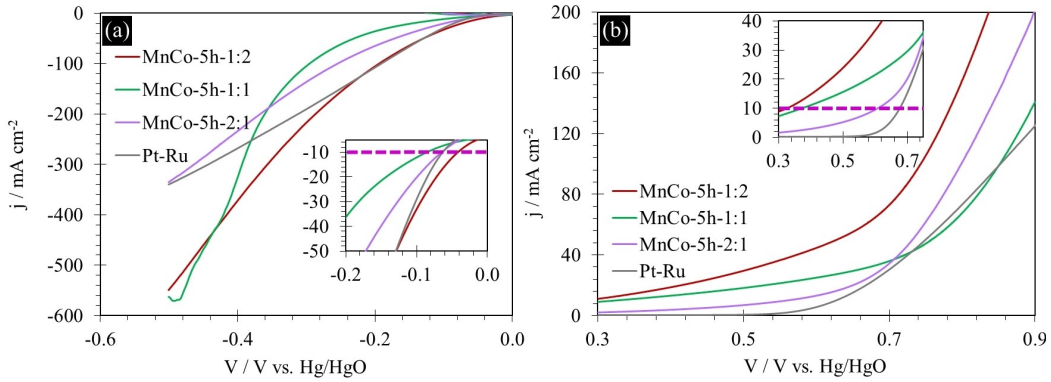

Figure 6. a) ORR and b) OER LSV half-cell test results at 5 mV cm^{-2} for different Mn:Co salt mass ratios and Pt–Ru.

absolute current density higher than MnCo-5h-2:1 and comparable to MnCo-5h-1:1. In fact, MnCo-5h-1:2 also has an absolute ORR onset potential slightly lower than that for Pt–Ru and a maximum absolute current density much higher than that for Pt–Ru (Table 4). MnCo-5h-2:1 has an OER onset potential that is comparable to Pt–Ru. All Mn–Co samples have better OER activity than Pt–Ru, both in terms on onset potential and maximum current density (Figure 6 and Table 4). MnCo-5h-1:2 has the lowest OER onset potential (0.28 V vs. Hg/HgO) and the highest maximum OER current density (293 mA cm^{-2}).

Table 4. ORR/OER onset potentials and maximum current densities for different Mn:Co salt ratios and Pt–Ru.

Sample	ORR onset potential [V vs. Hg/HgO]	OER onset potential [V vs. Hg/HgO]	Maximum ORR current density [mA cm^{-2}]	Maximum OER current density [mA cm^{-2}]
1:1	−0.08	0.32	−571	139
1:2	−0.04	0.28	−549	293
2:1	−0.06	0.56	−335	202
Pt-Ru	−0.06	0.63	−334	126

Research Article
doi.org/10.1002/batt.202100339
Chemistry Europe
European Chemical Societies Publishing

ZAB full-cell tests were done on the same 4 electrodes (Figure 7) and similar behavior to the half-cell tests was obtained. Efficiencies and potential gaps were calculated and are shown in Table 5. MnCo-5h-1:2 has a potential gap of 0.72 V and an efficiency of 63.7% at 10 mA cm^{-2}, while Pt–Ru has a potential gap of 0.77 V and an efficiency of 61.9% at the same current density. The potential gap for MnCo-5h-1:2 increases to 0.82 V and the efficiency decreases to 60.0% for a current density of 20 mA cm^{-2}. This performance is still better than that for Pt–Ru with an efficiency of 57.9% and a voltage gap of 0.88 V at 20 mA cm^{-2} (Table 5).

Because of its promising bifunctional catalytic performance, MnCo-5h-1:2 was chosen for further materials characterization (SEM/EDX) and electrochemical testing (cycling).

The SEM SE image and EDX maps for MnCo-5h-1:2 (Figure 8) show that the Mn–Co mixed oxide coating covers the entire surface of the fibers with some patches of thicker coating. EDX quantitative analysis, from different areas, gives a

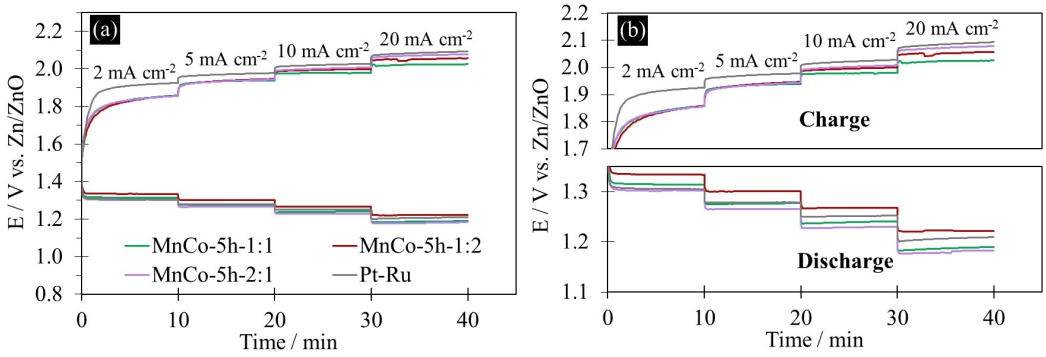

Figure 7. a) ZAB full-cell test results and b) enlarged view of full-cell test results for different Mn:Co salt ratios and Pt–Ru.

Table 5. Voltage gaps and efficiencies measured from full-cell tests for different Mn:Co salt ratios and Pt–Ru.

Sample	10 mA cm^{-2}		20 mA cm^{-2}	
	Voltage gap [V]	Efficiency [%]	Voltage gap [V]	Efficiency [%]
1:1	0.74	62.6	0.83	58.9
1:2	0.72	63.7	0.82	60.0
2:1	0.77	61.5	0.89	57.0
Pt-Ru	0.77	61.9	0.88	57.9

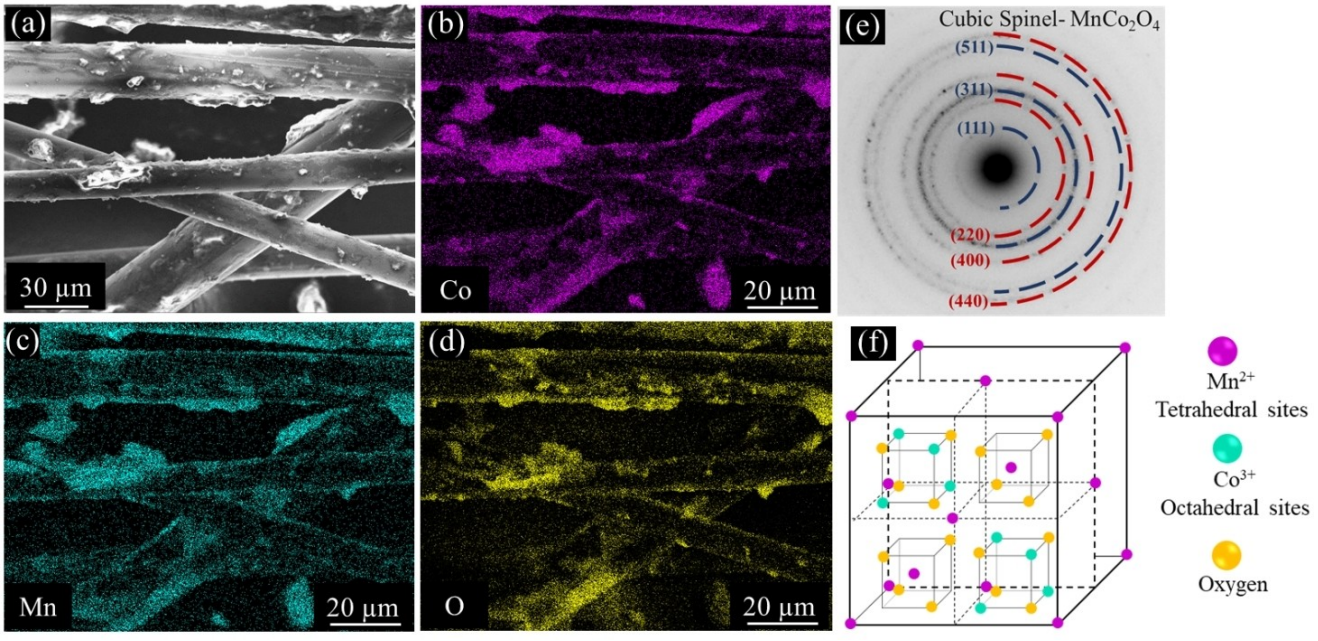

Figure 8. a) SEM, b–d) EDX and e) SAED analysis of MnCo-5h-1:2. f) Schematic of the spinel structure, showing some of the octahedral and tetrahedral sites.

Research Article
doi.org/10.1002/batt.202100339
Chemistry Europe
European Chemical Societies Publishing

Mn:Co atomic ratio of ~1:2, which corresponds to the Mn:Co salt ratio in the solution used for deposition. A representative SAED pattern is presented in Figure 8e and consists of concentric rings, which indicate that the oxide is polycrystalline. The pattern can be indexed to $MnCo_2O_4$ with a cubic spinel structure (PDF#23-1237, $a = 8.269$ Å). A schematic of the cubic spinel crystal structure is presented in Figure 8f, illustrating some of the tetrahedral and octahedral sites that act as active sites for O_2 donor-acceptor chemisorption. The tetrahedral cations fill 1/8 of the tetrahedral holes and the octahedral cations fill 1/2 of the octahedral holes.

The identification of the Mn–Co spinel phase was further confirmed through XPS analysis of MnCo-5h-1:2 (Figure 9). Figure 9a shows the survey spectrum; the Mn and Co peaks are from the coating, the C peak is from the CFs and the O peaks are from both the CFs and the Mn–Co oxide coating. The Na peak is likely from NaOH in the solution used for oxide coating and/or residual surface contamination. The peaks from the catalyst coating are relatively weak because of the small amount of catalyst compared with the carbon fibers.

High resolution spectra for Co and Mn are shown in Figure 9. The peak splitting for the Mn 3s spectrum (5.7 eV, Figure 9b) and the peak positions in the Mn 2p spectrum (Figure 9c) were used to estimate the Mn valence in the Mn–Co oxide spinel phase. Clark et al.[34] and Gorlin and Jaramillo[35] have demonstrated a relationship between Mn 3s peak splitting and the oxidation state of Mn. Based on these studies, the Mn 3s peak splitting of 5.7 eV corresponds to an oxidation state of 2+. The Mn 2p spectrum contains two main peaks that represent Mn $2p_{3/2}$ and Mn $2p_{1/2}$ at binding energies of 641.8 and 653.3 eV, respectively, which can be assigned to Mn^{2+}.[36–39] Deconvolution of the Co 2p spectrum leads to four components (Figure 9d). The peaks at binding energies of 780.7 and 796.5 eV correspond to Co $2p_{3/2}$ and Co $2p_{1/2}$, respectively.[40] The binding energies of the $2p_{3/2}$ and $2p_{1/2}$ shake-up satellite peaks were used to estimate the Co oxidation state. The satellite peak positions for Co $2p_{3/2}$ and $2p_{1/2}$ are 785.1 and 802.6 eV, respectively, which indicate the presence of Co^{3+} in MnCo-5h-1:2. From the XPS analysis results, it can be concluded that Mn and Co in the Mn–Co oxide coating have oxidation states of 2+ and 3+, respectively, rather than mixed oxidation states. This corresponds to a chemical formula for the spinel phase of $MnCo_2O_4$.

The good ORR/OER bifunctional catalytic activity of MnCo-5h-1:2 is proposed to be related to its spinel crystal structure (Figure 8e). The presence of both tetrahedral and octahedral sites (filled with Mn and Co cations, respectively) in the Mn–Co spinel structure provides donor-acceptor chemisorption sites (active sites) for O_2, which can provide efficient catalytic activity towards ORR/OER.[33]

The MnCo-5h-1:1 and MnCo-5h-2:1 samples were also characterized, using electron diffraction in the TEM and XPS (Figure SI1 and SI2). Both samples have SAED patterns similar to MnCo-5h-1:2 and the patterns can be indexed to a cubic spinel structure (Figure SI1a and b). High resolution XPS spectra for MnCo-5h-1:1 and MnCo-5h-2:1 are shown in Figure SI2a–f

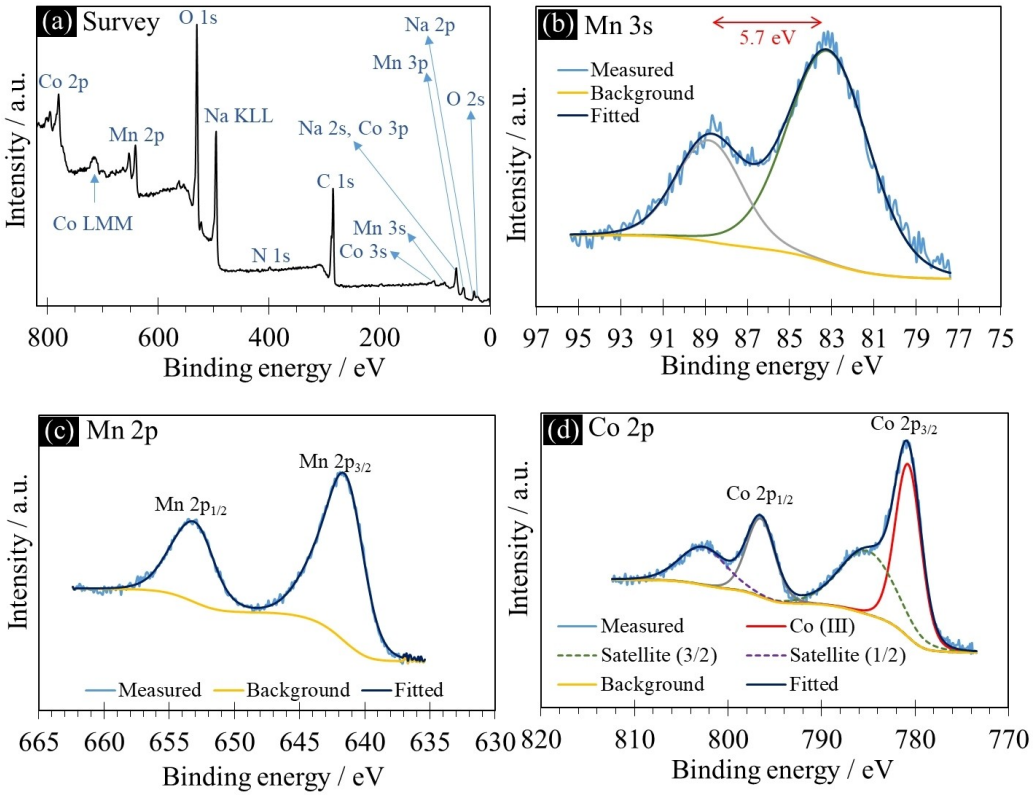

Figure 9. XPS analysis results for MnCo-5h-1:2. a) Overall survey spectrum, b) Co 2p spectrum, c) Mn 3s spectrum and d) Mn 2p spectrum.

Research Article
doi.org/10.1002/batt.202100339
Chemistry Europe
European Chemical Societies Publishing

and the oxidation states for Mn are summarized in Figure SI2g. The Mn oxidation state was determined from the Mn 3s peak splitting and 2p peak positions. Manganese in both samples has an overall oxidation state of ~2.6, which corresponds to a mixed of 2+ and 3+ valences. The Mn $2p_{3/2}$ spectrum can be deconvoluted into two components with binding energies of 641.2 eV (Mn^{2+}) and 642.8 eV (Mn^{3+}) for MnCo-5h-1:1 and 641.1 eV (Mn^{2+}) and 642.8 eV (Mn^{3+}) for MnCo-5h-2:1. The Co $2p_{3/2}$ spectra can be deconvoluted into two peaks at 780.4 eV (Co^{3+}) and 784.8 eV (Co^{2+}) for MnCo-5h-2:1 and 780.3 eV (Co^{3+}) and 784.8 eV (Co^{2+}) for MnCo-5h-1:1. In both MnCo-5h-2:1 and MnCo-5h-1:1, Mn and Co exist in the 2+ and 3+ oxidation states.[34,35]

The better catalytic activity for MnCo-5h-1:2, compared with MnCo-5h-1:1 and MnCo-5h-2:1, can be attributed to differences in the oxidation states. For MnCo-5h-1:2, Co exists exclusively in the 3+ state with Mn exclusively in the 2+ state. For both MnCo-5h-2:1 and MnCo-5h-1:1, Mn and Co have mixed oxidation states of 2+ and 3+.

In the $MnCo_2O_4$ spinel structure (MnCo-5h-1:2), Mn as Mn^{2+} occupies the tetrahedral sites and Co as Co^{3+} occupies the octahedral sites. In the MnCo-5h-1:1 and MnCo-5h-2:1 spinel structures, the tetrahedral and octahedral sites are occupied by both Mn^{2+} and Co^{2+}. It is proposed that a Mn–Co mixed oxide electrocatalyst with a spinel crystal structure, with Mn in the 2+ oxidation state and Co in the 3+ state (MnCo-5h-1:2), has better bifunctional catalytic activity than a spinel structure where Mn and Co both have mixed oxidation states of 2+ and 3+ (MnCo-5h-2:1 and MnCo-5h-1:1). There are conflicting reports in the literature regarding oxidation state and catalytic activity. Some recent papers indicate that higher oxidation states for Mn (3+/4+) lead to better ORR catalytic activity, e.g., the work by Li et al.[41] and the study by We et al.[42] On the other hand, there are other recent studies, e.g., Cheng et al.,[43] that show that a lower Mn oxidation state is preferred for ORR catalytic activity. In any case, for the samples in this study, the combination of Mn^{2+} and Co^{3+} provided superior bifunctional catalytic activity. It is also noteworthy that most recent articles claim that the presence of Co^{3+} in the spinel structure is beneficial in terms of OER performance.[44]

The cycling performance of batteries prepared using MnCo-5h-1:2 and Pt–Ru as the air electrodes and a zinc sheet (2× 6 cm) as the counter electrode was tested at a current density of 10 mA cm^{-2} for 200 charge/discharge cycles. This corresponds to a total cycling time of 100 h with charge and discharge durations of 10 min each and a 5 min rest period after each charge and discharge step (Figure 10). During the first 4 cycles, the ORR potential decreases and the OER potentials increases slightly for MnCo-5h-1:2. This may be due to oxidation of the CFs upon exposure to the alkaline electrolyte.[31] MnCo-5h-1:2 cycling performance is very stable without any major fluctuations during subsequent cycles, with initial discharge and charge potentials of 1.27 V vs. Zn/ZnO and 1.99 V vs. Zn/ZnO, respectively, and final values after 200 cycles of 1.22 V vs. Zn/ZnO and 2.02 V vs. Zn/ZnO, (Figure 10c). The initial efficiency is 63.7% and the final efficiency is 58.9%, which corresponds to only a 7.5% decrease in efficiency. The electrode with Pt–Ru is not stable during cycling with initial and final efficiencies of 61.9% and 43.2%, respectively, after 200 cycles, which represents a 30.2% drop in efficiency. A power curve comparison for MnCo-5h-1:2 and Pt–Ru is presented in Figure 10d. The power curve for MnCo-5h-1:2

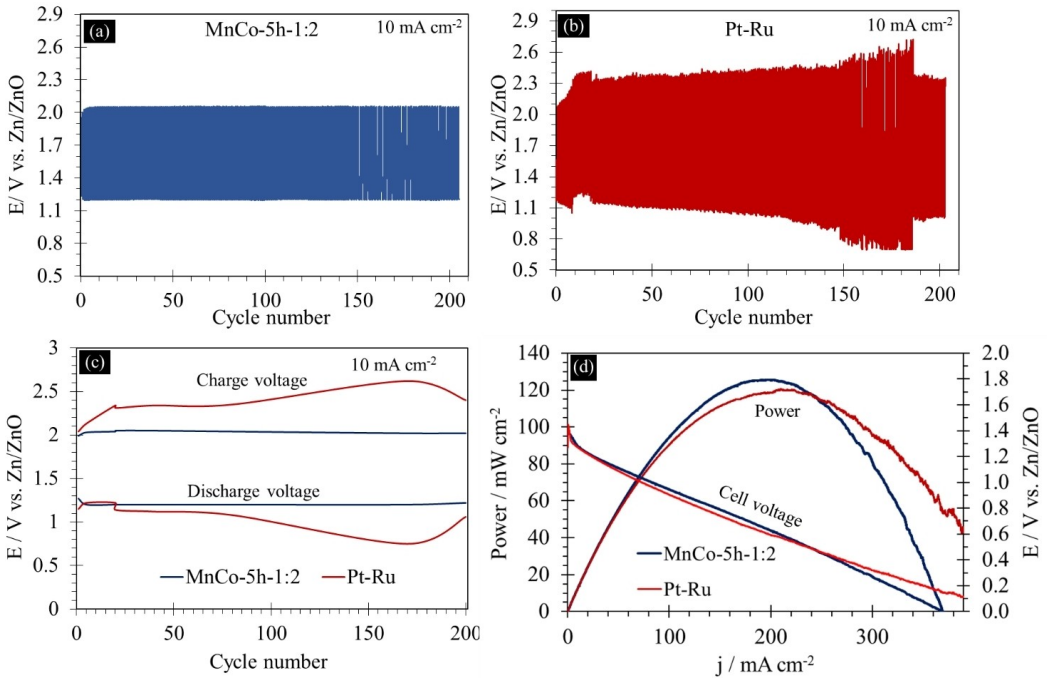

Figure 10. Cycling tests at 10 mA cm^{-2} for a) MnCo-5h-1:2 and b) Pt–Ru. c) Charge and discharge potentials for both cells during cycling. d) Polarization and power comparison.

Research Article
doi.org/10.1002/batt.202100339
Chemistry Europe
European Chemical Societies Publishing

reaches a maximum power density of 127 mW cm^{-2} at 198 mA cm^{-2} which is slightly better than the maximum power density of 121 mW cm^{-2} for Pt–Ru at 223 mA cm^{-2}.

MnCo-5h-1:2 electrodes were characterized using SEM/EDX analysis before and after cycling (Figure 11). SEM SE images (Figure 11a–c) and K maps (Figure 11e and f) for the electrodes after 10 and 200 cycles show that K coverage, likely in the form of potassium carbonate, increases with cycling. However, battery performance was not adversely affected as there was very little change from the 10th to the 200th cycle. This is due in part to the size of the carbon fibers (~10 μm in diameter) which results in a more open air electrode with relatively large voids and pores that are visible to the human eye (Figure 11a–c). The large voids aid oxygen delivery and removal during ORR and OER when the battery is discharged or charged, leading to stable cycling behavior. Oxidation of carbon fibers and carbon black added during electrode fabrication is likely responsible for the small performance degradation during the initial cycles. After 200 cycles, the amount of Mn and Co from the EDX analysis (Figure 11d) decreases due to the increased coverage of K; however, the Mn:Co ratio remains approximately constant. There is a small amount of Zn on the surface of the cycled electrodes, as ZnO, and this is likely due to the presence of soluble zincate [$Zn(OH)_4^{2-}$] species in the electrolyte.

It is apparent that MnCo-5h-1:2 is very stable as a bifunctional catalyst after cycling at 10 mA cm^{-2} for 200 cycles. Furthermore, the performance of MnCo-5h-1:2 is superior to that of other bifunctional transition metal oxide/carbon-based catalysts reported in the recent literature (Table 6). As an example, Co–Mn–Ni nanorods were prepared by Wang et al.

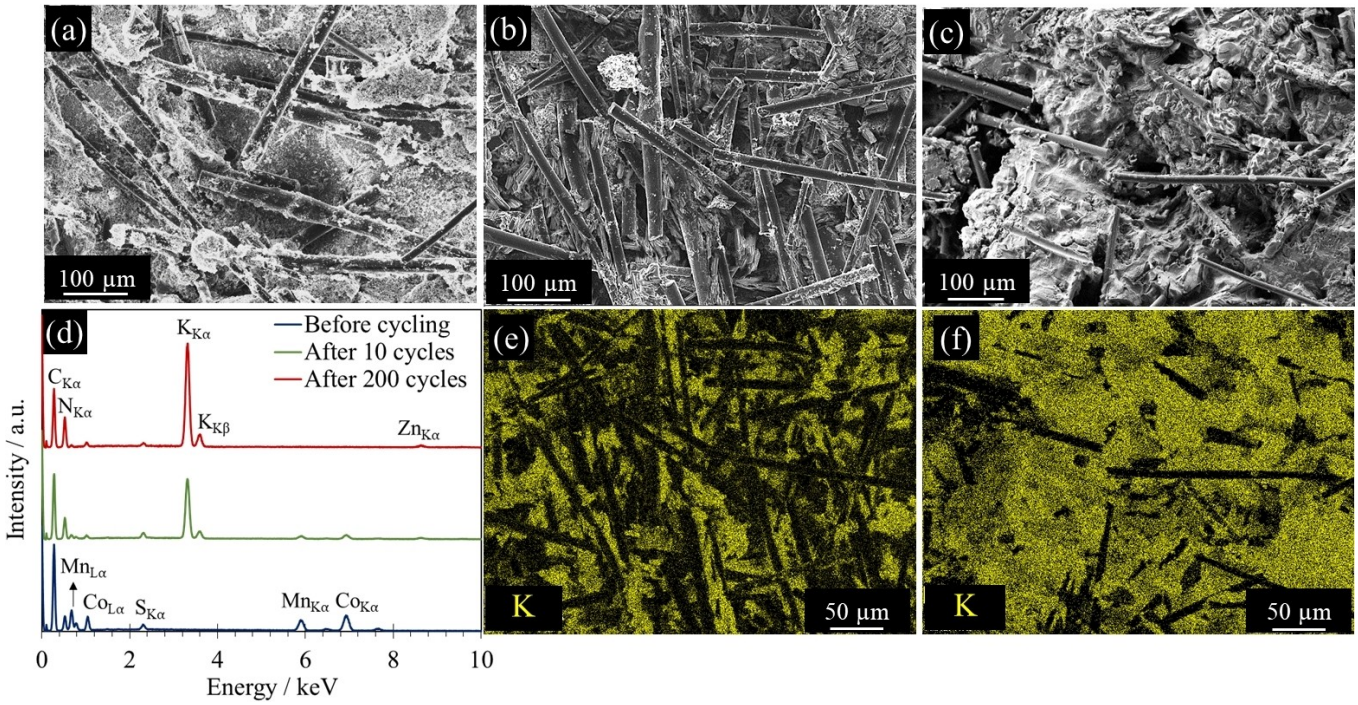

Figure 11. SEM images and EDX analysis of MnCo-5h-1:2 electrodes before and after battery cycling. a) SE image before cycling, b) SE image after 10 cycles, c) SE image after 200 cycles, d) EDX spectra from the areas shown in the SEM images, e) K EDX map for the electrode after 10 cycles and f) K EDX map for the electrode after 200 cycles.

Table 6. Comparison of bifunctional transition metal oxide/carbon-based catalysts recently reported in the literature.

Catalyst/air electrode material	Battery/cell characterization	Cycling current density, *j* [mA cm^{-2}]	Initial efficiency	Final efficiency	Number of cycles, cycling duration [h]
$MnCo_2O_4$/CF (this work)	6 M KOH + 0.25 M ZnO, ambient air	10	63.7	58.9	200, 100
Co–Mn–Ni nanorods[38]	6 M KOH + 0.2 M $Zn(Ac)_2$, ambient air	10	–	57.4	100, 16.7
MnO_x + CoFe on GDL[2]	6 M KOH + 0.25 M ZnO, ambient air	10	59	57	200, 100
$(Co,Fe)_3O_4$/CNT on GDL[45]	6 M KOH + 0.25 M ZnO, ambient air	10	59.1	58.5	200, 100
Co-Fe[19]	6 M KOH + 0.25 M ZnO, ambient air	5	~56	~56	20, 20
$NiCo_2O_4$ on Ni-GDL[46]	6 M KOH, ambient air	10	~59.1	Battery failed after 75 cycles	100, 100

and cycled in a ZAB containing 6 M KOH + 0.2 M $Zn(Ac)_2$ electrolyte at 10 mA cm^{-2}.[38] Only final efficiency values were provided in their work, but a significant increase in the OER potential and a decrease in the ORR potential were reported. Aasen et al. prepared $(Co,Fe)_3O_4$/CNT bifunctional catalysts on GDL that were cycled at both 10 and 20 mA cm^{-2} in 6 M KOH + 0.25 M ZnO.[45] The reported cycling performance was quite stable; however, ORR/OER half-cell catalytic activities for MnCo-5h-1:2 in this work are superior. In addition, synthesis of MnCo-5h-1:2 is more cost-effective since no costly carbonaceous precursors like CNTs are required. Another example is the work by Cano et al., where $NiCo_2O_4$ catalysts on a Ni-based GDL were prepared and cycled in 6 M KOH at 10 mA cm^{-2}.[46] However, significant performance losses were reported after 50 h of cycling (~55.6% efficiency). Performance then declined more rapidly until 100 h with a final discharge potential of ~0.1 V vs. Zn/ZnO. The discharge potential for MnCo-5h-1:2 is 1.19 V vs. Zn/ZnO after 200 cycles.

3. Conclusions

Highly stable and efficient Mn–Co oxide/carbon fiber bifunctional catalyst/air electrodes were synthesized through a facile and cost-effective method. Asphaltene as a by-product of the oil sands industry was used to prepare carbon fibers (CFs) which were then coated with Mn–Co oxide, identified as cubic spinel $MnCo_2O_4$, via a simple sonication method as the bifunctional catalyst. Several sonication times and Mn:Co ratios were examined in terms of their catalytic activity towards ORR/OER, charge/discharge efficiencies in full-cell Zn-air batteries and cycling behavior. A sonication time of 5 h with a Mn:Co ratio of 1:2 provided the best performance. The ORR onset potential for this sample (MnCo-5h-1:2), measured from LSV tests in a half-cell (three electrode) configuration, was −0.04 V vs. Hg/HgO with a maximum current density of −549 mA cm^{-2}. Its activity towards OER was also outstanding with an OER onset potential of 0.28 V vs. Hg/HgO and a maximum current density of 293 mA cm^{-2}. Discharge/charge efficiencies for MnCo-5h-1:2 were 63.7% and 60.0% at 10 and 20 mA cm^{-2}, respectively. MnCo-5h-1:2 was very stable during cycling at 10 mA cm^{-2}, without any major fluctuations in discharge/charge potentials and a final efficiency of 58.9% (after 200 cycles). The cycling performance was also superior to that of Pt–Ru electrodes, which had initial and final efficiencies of 61.9% and 43.2%, respectively, under the same conditions. The excellent battery performance is proposed to be due to the inherent ORR/OER bifunctional activity of Mn–Co mixed oxides and its direct and intimate growth on the CFs.

Acknowledgements

This work was financially supported by Alberta Innovates (Canada) through the Bitumen Beyond Combustion program and the Natural Sciences and Engineering Research Council (NSERC) of Canada.

Conflict of Interest

The authors declare no conflict of interest.

Data Availability Statement

The data that support the findings of this study are available from the corresponding author upon reasonable request.

Keywords: bifunctional electrocatalyst · carbon fiber · efficient · $MnCo_2O_4$ · zinc-air battery

[1] P. Pei, K. Wang, Z. Ma, *Appl. Energy* **2014**, *128*, 315–324.
[2] M. P. Clark, M. Xiong, K. Cadien, D. G. Ivey, *ACS Appl. Energ. Mater.* **2020**, *3*, 603–613.
[3] J. Park, M. Park, G. Nam, J. Lee, J. Cho, *Adv. Mater.* **2015**, *27*, 1396–1401.
[4] J. Pan, X. L. Tian, S. Zaman, Z. Dong, H. Liu, H. S. Park, B. Y. Xia, *Batteries & Supercaps* **2019**, *2*, 336–347; Supercaps **2019**, 2, 336–347.
[5] P. Gu, M. Zheng, Q. Zhao, X. Xiao, H. Xue, H. Pang, *J. Mater. Chem. A* **2017**, *5*, 7651–7666.
[6] S. Müller, F. Holzer, O. Haas, *J. Appl. Electrochem.* **1998**, *28*, 895–898.
[7] L. Pan, D. Chen, P. Pei, S. Huang, P. Ren, X. Song, *Appl. Energy* **2021**, *290*, 116777.
[8] K. Akbarzadeh, A. Hammami, A. Kharrat, D. Zhang, S. Allenson, J. Creek, S. Kabir, A. Jamaluddin, A. G. Marshall, R. P. Rodgers, O. C. Mullins, T. Solbakken, *Oilfield Rev.* **2007**, *19*, 22–43.
[9] ST53, (n.d.). https://www.aer.ca/providing-information/data-and-reports/statistical-reports/st53.html.
[10] S. Alimohammadi, S. Zendehboudi, L. James, *Fuel* **2019**, *252*, 753–791.
[11] J. S. Lee, S. T. Kim, R. Cao, N. S. Choi, M. Liu, K. T. Lee, J. Cho, *Adv. Energy Mater.* **2011**, *1*, 34–50.
[12] J. Suntivich, H. A. Gasteiger, N. Yabuuchi, H. Nakanishi, J. B. Goodenough, Y. Shao-Horn, *Nat. Chem.* **2011**, *3*, 546–550.
[13] S. Yang, Y. Cheng, X. Xiao, H. Pang, *Chem. Eng. J.* **2020**, *384*, 123294.
[14] F. Cheng, J. Chen, *Chem. Soc. Rev.* **2012**, *41*, 2172–2192.
[15] M. P. Clark, T. Muneshwar, M. Xiong, K. Cadien, D. G. Ivey, *ACS Appl. Nano Mater.* **2019**, *2*, 267–277.
[16] Z. Abedi, D. Leistenschneider, W. Chen, D. G. Ivey, *Energy Technol.* **2020**, *2000588*, 1–11.
[17] M. Wu, Y. Wang, Z. Wei, L. Wang, M. Zhuo, J. Zhang, X. Han, J. Ma, *J. Mater. Chem. A* **2018**, *6*, 10918–10925.
[18] L. Wang, Y. Wang, M. Wu, Z. Wei, C. Cui, M. Mao, *Small* **2018**, *14*, 1800737.
[19] M. Xiong, D. G. Ivey, *Electrochem. Commun.* **2017**, *75*, 73–77.
[20] Z. C. Yao, T. Tang, J. S. Hu, L. J. Wan, *Energy Fuels* **2021**, *35*, 6380–6401.
[21] J. M. Costa, M. P. Clark, A. F. de Almeida Neto, D. G. Ivey, *Int. J. Hydrogen Energy* **2020**, *45*, 16122–16132.
[22] Y. Li, J. Lu, *ACS Energy Lett.* **2017**, *2*, 1370–1377.
[23] P. Zuo, D. Leistenschneider, Y. Kim, Z. Abedi, D. G. Ivey, X. Zhang, W. Chen, *J. Ind. Eng. Chem.* **2021**, *104*, 427–436.
[24] D. Leistenschneider, P. Zuo, Y. Kim, Z. Abedi, D. G. Ivey, A. D. Klerk, W. Chen, *Carbon Trends* **2021**, *5*, 100090.
[25] L. Li, J. Yang, H. Yang, L. Zhang, J. Shao, W. Huang, B. Liu, X. Dong, *ACS Appl. Energ. Mater.* **2018**, *1*, 963–969.
[26] N. Borchers, S. Clark, B. Horstmann, K. Jayasayee, M. Juel, P. Stevens, *J. Power Sources* **2021**, *484*, 229309.
[27] A. Sayah, F. Habelhames, A. Bahloul, B. Nessark, *J. Electroanal. Chem.* **2018**, *818*, 26–34.
[28] B. N. Liu, F. Luo, H. Wu, Y. Liu, C. Zhang, J. Chen, *Adv. Funct. Mater.* **2008**, *18*, 1518–1525.
[29] O. Fromm, A. Heckmann, U. C. Rodehorst, J. Frerichs, D. Becker, M. Winter, T. Placke, *Carbon* **2018**, *128*, 147–163.
[30] L. Qu, Y. Liu, J. Baek, L. Dai, *ACS Nano* **2010**, *4*, 1321–1326.
[31] P. N. Ross, M. Sattler, *J. Electrochem. Soc.* **1988**, *135*, 1464.
[32] H. W. Zhang, Y. X. Lu, B. Li, G. F. Huang, F. Zeng, Y. Y. Li, A. Pan, Y. F. Chai, W. Q. Huang, *J. Mater. Sci. Technol.* **2021**, *86*, 210–218.
[33] A. K. Worku, D. W. Ayele, N. G. Habtu, M. A. Teshager, Z. G. Workineh, *Mater. Today Sustain.* **2021**, *13*, 100072.

[34] M. P. Clark, W. Qu, D. G. Ivey, *J. Appl. Electrochem.* **2017**, *47*, 39–49.
[35] Y. Gorlin, T. F. Jaramillo, *J. Am. Chem. Soc.* **2010**, *132*, 13612–13614.
[36] W. Wang, L. Kuai, W. Cao, M. Huttula, S. Ollikkala, T. Ahopelto, A. P. Honkanen, S. Huotari, M. Yu, B. Geng, *Angew. Chem. Int. Ed.* **2017**, *56*, 14977–14981; *Angew. Chem.* **2017**, *129*, 15173–15177.
[37] M. C. Biesinger, B. P. Payne, A. P. Grosvenor, L. W. M. Lau, A. R. Gerson, R. S. C. Smart, *Appl. Surf. Sci.* **2011**, *257*, 2717–2730.
[38] Q. Wang, Y. Xue, S. Sun, S. Yan, H. Miao, Z. Liu, *J. Power Sources* **2019**, *435*, 226761.
[39] E. S. Ilton, J. E. Post, P. J. Heaney, F. T. Ling, S. N. Kerisit, *Appl. Surf. Sci.* **2016**, *366*, 475–485.
[40] H. Su, X. Wang, J. Hu, T. Ouyag, K. Xiao, Z. Liu, *J. Mater. Chem. A* **2019**, *7*, 22307–22313.
[41] K. Li, R. Zhang, R. Gao, G. Shen, L. Pan, Y. Yao, *Appl. Catal. B* **2019**, *244*, 536–545.
[42] C. Wei, Z. Feng, G. G. Scherer, J. Barber, Y. Shao-Horn, Z. J. Xu, *Adv. Mater.* **2017**, *29*, 1–8.
[43] F. Cheng, T. Zhang, Y. Zhang, J. Du, X. Han, J. Chen, *Angew. Chem. Int. Ed.* **2013**, *52*, 2474–2477; *Angew. Chem.* **2013**, *125*, 2534–2537.
[44] Y. Sun, S. Gao, F. Lei, J. Liu, L. Liang, Y. Xie, *Chem. Sci.* **2014**, *5*, 3976–3982.
[45] D. Aasen, M. P. Clark, D. G. Ivey, *Batteries & Supercaps* **2020**, *3*, 174–184; Supercaps **2020**, 3, 174–184.
[46] Z. P. Cano, M. G. Park, D. U. Lee, J. Fu, H. Liu, M. Fowler, Z. Chen, *J. Phys. Chem. C* **2018**, *122*, 20153–20166.

Manuscript received: November 11, 2021
Accepted manuscript online: November 19, 2021
Version of record online: December 2, 2021